

Riemannian geometry study of vapor-liquid phase equilibria and supercritical behavior of the Lennard-Jones fluid

Helge-Otmar May

University of Applied Sciences, Darmstadt, Germany

Peter Mausbach

Cologne University of Applied Sciences, Cologne, Germany

(Received 21 December 2011; published 5 March 2012)

The behavior of thermodynamic response functions and the thermodynamic scalar curvature in the supercritical region have been studied for a Lennard-Jones fluid based on a revised modified Benedict-Webb-Rubin equation of state. Response function extrema are sometimes used to estimate the Widom line, which is characterized by the maxima of the correlation lengths. We calculated the Widom line for the Lennard-Jones fluid without using any response function extrema. Since the volume of the correlation length is proportional to the Riemannian thermodynamic scalar curvature, the locus of the Widom line follows the slope of maximum curvature. We show that the slope of the Widom line follows the slope of the isobaric heat capacity maximum only in the close vicinity of the critical point and that, therefore, the use of response function extrema in this context is problematic. Furthermore, we constructed the vapor-liquid coexistence line for the Lennard-Jones fluid using the fact that the correlation length, and therefore the thermodynamic scalar curvature, must be equal in the two coexisting phases. We compared the resulting phase envelope with those from simulation data where multiple histogram reweighting was used and found striking agreement between the two methods.

DOI: [10.1103/PhysRevE.85.031201](https://doi.org/10.1103/PhysRevE.85.031201)

PACS number(s): 51.30.+i, 61.20.-p, 05.70.-a, 64.10.+h

I. INTRODUCTION

Supercritical fluids are widely used in industrial processes like extraction and separation. Their behavior away from the critical point is therefore an important practical question because it might affect their applicability in the considered technological process. Therefore, the localization and physico-chemical interpretation of the extrema of thermodynamic properties have been the subject of many investigations [1–5].

Fluids in their supercritical state are both dense and compressible, and it is commonly said that there is no difference between a liquid and a gas state. The thermodynamic properties of supercritical fluids vary continuously with changes in pressure or temperature. However, supercritical fluids exhibit peculiar properties that are sometimes similar to those of gases and sometimes to those of liquids. In the vicinity of the critical point, several thermodynamic response functions show extrema when the pressure or temperature is changed. The lines of these extrema form a whole set of “ridges” in the phase space and can be regarded as extensions of the vapor-liquid coexistence line into the supercritical region. In contrast to the traditional picture of supercritical fluids, Simeoni *et al.* [6] recently discussed how the locus of the maxima of the correlation length ξ for thermodynamic fluctuations, i.e., the Widom line, could be considered as a boundary that separates the supercritical region into gaslike and liquidlike regions. Because of the lack of a theoretical method for the construction of the Widom line, the locus of extrema of the constant-pressure specific heat c_p was used as an estimation for the Widom line. Different dynamic regimes in supercritical argon were identified on crossing the estimated Widom line. In a different study [7], the maxima of the isothermal compressibility β_T , thermal expansion coefficient α_p , and heat capacity c_p were used to estimate the Widom line

of a Lennard-Jones (LJ) system. Since the lines of maxima should merge into one line near the critical point, the three lines were thought to coincide if the temperature of the different lines differed by less than 1%. However, in both studies, the estimation of the Widom line is unsatisfactory because it is *a priori* unclear how far from the critical point the lines of extrema of response functions follow the exact Widom line. It is worth noting that especially in the temperature-density projection of the phase space, a rapid widening of the bunch of extrema lines can be observed upon departure from the critical point.

Fortunately, in a very recent study Ruppeiner *et al.* [8] proposed a construction of the Widom line by using a novel approach based on Riemannian geometry. Ruppeiner [9] established a connection between the Riemannian thermodynamic scalar curvature R of the thermodynamic metric and the volume of the correlation length ξ , to wit, $|R| \propto \xi^3$. Consequently, the locus of the maximum of $|R|$ describes the locus of the Widom line.

Moreover, Ruppeiner *et al.* could describe how the vapor-liquid phase transition can be calculated by using the fact that the correlation length ξ must be the same in the two coexisting phases. Thus, the first-order vapor-liquid phase transition curve can be estimated from the equality of R calculated in the two coexisting phases. Ruppeiner *et al.* called the procedure the R -crossing method and applied it to a van der Waals (vdW) fluid [8]. It is of great interest to apply this approach to a more realistic system, such as a LJ fluid. The concept of Riemannian geometry provides the first theoretical construction of the Widom line without the need for any thermodynamic response function and a novel way of characterizing first-order phase transitions.

In order to obtain accurate predictions for the LJ fluid, we used a phenomenological equation of state (EOS) obtained

by means of a modified Benedict-Webb-Rubin (MBWR) equation [10,11] in our study. There are other high-quality EOSs for the LJ fluid, but we used this MBWR EOS because it was the most commonly quoted EOS in the literature. Using extensive simulation data for a LJ fluid at 348 state points from the thesis of Meier [12], we recalculated the multiparameter MBWR EOS. Meier's data were the best data we could find for the LJ fluid concerning the density of state points and the quality. From this accurate analytical EOS, we then constructed the loci of extrema at constant pressure and temperature for the isothermal compressibility β_T , the thermal expansion coefficient α_p , and the isobaric heat capacity c_p .

It was shown elsewhere [13] that the use of different ansatz functions in an EOS can cause different courses of the extremal lines. To validate the revised MBWR EOS, we compared our results with those of another high-quality EOS, the Kolafa-Nezbeda (KN) equation [14] which uses a different ansatz. The overall agreement between the two equations is very good for the entire range of density and temperature, and both equations indicate different results from those recently published [7] in which the line of extrema for the isobaric heat capacity approaches the critical isochore when the temperature is increased. Brazhkin *et al.* [7] concluded from this that a vdW fluid represents a fairly universal behavior of the Widom line for a liquid-gas transition, in which the locus of constant-pressure specific heat extrema exactly follows the critical isochore [15]. Our results for the LJ fluid are different.

Based on the MBWR EOS, we calculated the state point dependence of the Riemannian thermodynamic scalar curvature R for a large region in phase space. This is interesting because R carries information about the interaction of the fluid system [16,17]. Using R , we then calculated the course of the Widom line for a LJ fluid and we showed that only the extrema of constant-pressure specific heat c_p follow the Widom line in the close vicinity of the critical point.

Finally, we calculated the vapor-liquid coexistence line by using the R -crossing method of Ruppeiner *et al.* [8]. We compared our results to those obtained by Shi and Johnson [18], who used multiple histogram reweighting to compute the phase envelope. We can show that the overall agreement between the two methods is very good.

II. A REVISED MBWR EQUATION OF STATE

The MBWR EOS with 33 adjustable parameters has been used successfully by Nicolas *et al.* [10] and by Johnson *et al.* [11] to fit the thermodynamic data of a LJ fluid, and by others to fit the data of a core-softened fluid [19]. Most of the fitting data of Johnson *et al.* belonged to the supercritical region. In Meier's thesis [12], the thermodynamic simulation data of a LJ fluid for a large number of additional state points are given. We used Meier's data to calculate the parameters of the MBWR EOS. The EOS for the pressure p as a function of density ρ and temperature T is formulated with 32 linear parameters x_i and one nonlinear parameter γ :

$$p(\rho, T) = \rho T + \rho^2(x_1 T + x_2 T^{1/2} + x_3 + x_4 T^{-1} + x_5 T^{-2}) \\ + \rho^3(x_6 T + x_7 + x_8 T^{-1} + x_9 T^{-2}) \\ + \rho^4(x_{10} T + x_{11} + x_{12} T^{-1})$$

$$+ \rho^5 x_{13} + \rho^6(x_{14} T^{-1} + x_{15} T^{-2}) + \rho^7(x_{16} T^{-1}) \\ + \rho^8(x_{17} T^{-1} + x_{18} T^{-2}) + \rho^9(x_{19} T^{-2}) \\ + \exp(-\gamma \rho^2)[\rho^3(x_{20} T^{-2} + x_{21} T^{-3}) \\ + \rho^5(x_{22} T^{-2} + x_{23} T^{-4}) + \rho^7(x_{24} T^{-2} + x_{25} T^{-3}) \\ + \rho^9(x_{26} T^{-2} + x_{27} T^{-4}) + \rho^{11}(x_{28} T^{-2} + x_{29} T^{-3}) \\ + \rho^{13}(x_{30} T^{-2} + x_{31} T^{-3} + x_{32} T^{-4})]. \quad (1)$$

We used normal conventions for all reduced LJ parameters [11]: The reference density is m/σ^3 where m is the particle mass and σ is the LJ atomic diameter; the reference pressure is ε/σ^3 where ε is the LJ well depth, which is the reference energy; ε/k_B is the reference temperature where k_B is Boltzmann's constant. All quantities quoted in this work are in terms of the reduced quantities. Unless otherwise noted, all thermodynamic functions will be considered as functions of density and temperature in the following. The residual (configurational) internal energy u^E which is a reduced energy per particle is related to the pressure by

$$u^E = \int_0^\rho \left(p - T \frac{\partial p}{\partial T} \right) \frac{d\rho}{\rho^2}. \quad (2)$$

Our procedure for calculating the unknown parameters is similar to the description given elsewhere [11,19] and will therefore not be repeated here. We explicitly make use of critical point data obtained from Shi and Johnson [18] in the course of our fitting procedure. We used the critical values of $\rho_c = 0.316$ and $T_c = 1.3145$ for a long-range corrected potential with a reduced cutoff value of 5.0. The nonlinear parameter is set to $\gamma = 3$; compare Johnson *et al.* [11]. The first five parameters x_1 – x_5 are the same as in this paper [11]; they were generated from exact second virial coefficients. The remaining parameters were calculated with Meier's data without weighting because no uncertainties for pressure and energy are given in Meier's thesis. The final values of the 32 parameters x_i are presented in Table I.

In Fig. 1(a), the density dependence of the pressure at different constant temperatures ranging from 1.1 to 6 is shown;

TABLE I. New parameters for the MBWR EOS regressed from Meier's data [12].

i	x_i	i	x_i
1	0.862 308 509 750 7421	17	−12 849.646 945 560 7240
2	2.976 218 765 822 098	18	9.969 125 083 269 407 38
3	−8.402 230 115 796 038	19	−163 99.834 972 062 1627
4	0.105 413 662 920 3555	20	−256.926 076 715 047 884
5	−0.856 458 382 817 4598	21	−145 88.020 393 359 6368
6	1.447 873 188 137 063 22	22	−12 849.646 945 560 7240
7	−0.310 267 527 929 454 501	23	9.969 125 083 269 407 38
8	3.267 007 738 566 634 08	24	−16 399.834 972 062 1627
9	4402.402 104 295 189 02	25	−256.926 076 715 047 884
10	0.016 537 538 935 922 5696	26	−14 588.020 393 359 636
11	7.421 502 018 692 505 59	27	88.308 296 074 852 1799
12	−40.796 710 691 412 2298	28	−6417.298 420 881 501 44
13	16.453 782 538 214 1350	29	121.307 436 784 732 417
14	12.838 907 122 793 5610	30	−4461.883 327 409 137 56
15	−1407.065 802 596 428 97	31	−507.183 302 372 831 804
16	−33.225 173 894 770 5988	32	37.238 579 454 630 5178

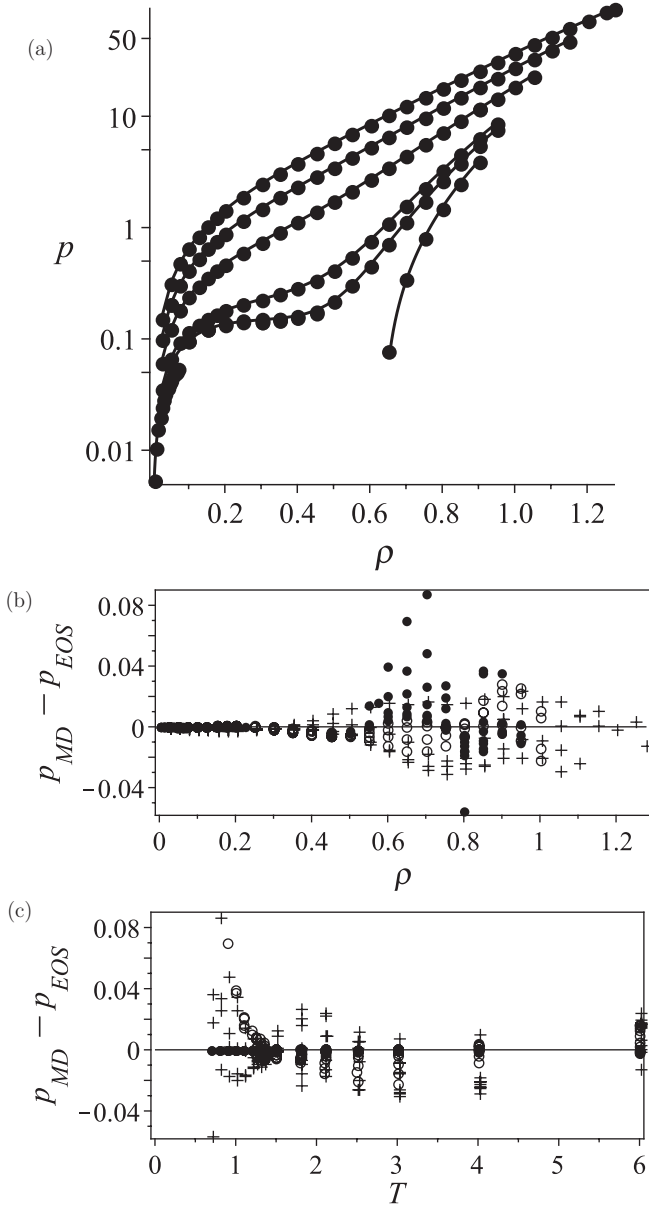


FIG. 1. (a) Comparison between simulated pressure data and EOS at different constant temperatures; here symbols represent Meier's simulation data [12] and continuous lines are calculated from the refit of the MBWR EOS. $T = 6.0, 4.0, 2.5, 1.5, 1.35$, and 1.1 (from top to bottom). (b),(c) Deviation plots for pressure, where p_{MD} denotes Meier's simulation data [12] and p_{EOS} denotes the MBWR EOS calculation. In (b) the solid circles are for $T < T_c$, the open circles are for $T_c < T < 2.5$, and the crosses are for $T \geq 2.5$. In (c) the solid circles are for $\rho < 0.2$, the circles are for $0.2 < \rho < 0.5$, and the crosses are for $\rho \geq 0.5$.

symbols represent the simulation data of Meier [12] and continuous lines are calculated from our current fit of the MBWR EOS. The overall agreement for the entire range of density and temperature is good. In Figs. 1(b) and 1(c) we show the deviations for the pressure, $p_{MD} - p_{EOS}$, where p_{MD} denotes Meier's simulation data [12] and p_{EOS} is calculated from the MBWR EOS. The deviations are much smaller than in [11]; this is an argument for the quality of the simulation

data of Meier, and we believe that our revised MBWR EOS can be used properly for further analysis.

III. LINES OF EXTREMA OF THERMODYNAMIC RESPONSE FUNCTIONS

In previous work [6,7], the extrema of thermodynamic response functions were used for an estimation of the Widom line. In order to study their relation to the exact Widom line, we have calculated the maxima of the thermal expansion coefficient

$$\alpha_p = \frac{\frac{\partial p}{\partial T}}{\rho \frac{\partial p}{\partial \rho}}, \quad (3)$$

the isobaric heat capacity

$$c_p = \frac{T \left(\frac{\partial p}{\partial T} \right)^2}{\rho^2 \frac{\partial p}{\partial \rho}} + \frac{\partial u}{\partial T}, \quad (4)$$

and the isothermal compressibility β_T from

$$1/\beta_T = \rho \frac{\partial p}{\partial \rho} \quad (5)$$

for both constant temperature and constant pressure. The density dependence of these quantities is given in Fig. 2. In the left column we show results at constant temperature and in the right column at constant pressure.

The response functions exhibit a strong increase in the vicinity of the critical point; therefore all response functions are plotted logarithmically in Fig. 2. The maximum of the isothermal compressibility β_T at constant temperature vanishes quickly in the supercritical region, whereas the maxima of the thermal expansion coefficient α_p and of the isobaric heat capacity c_p also exist at higher temperatures.

The extrema of the curves in Fig. 2 determine the lines of response function maxima in Fig. 3 where the ρ - T projection [Fig. 3(a)] and the p - T projection [Fig. 3(b)] of the lines at constant temperature are shown; the corresponding courses of lines at constant pressure are given in Figs. 3(c) and 3(d). The lines of the maxima of β_T at constant temperature [Fig. 3(a)] and at constant pressure [Fig. 3(c)] correspond in both cases to a decrease in the density with temperature increase. The same is true for the line of the α_p maxima at constant temperature [Fig. 3(a)], whereas the line of the α_p maxima at constant pressure [Fig. 3(c)] corresponds to an increase in density with temperature increase before $\alpha_{p,max}$ passes through a maximum at about $\rho = 1.75\rho_c$. Except in the vicinity of the critical point, the line of c_p maxima at constant temperature [Fig. 3(c)] runs away from the critical isochore. It should be mentioned that the description of the thermodynamic behavior in the close vicinity of the critical point based on the MBWR EOS is uncertain. However, an interesting result of this presentation is that the c_p line of maxima at constant temperature [Fig. 3(a)] does not turn back to the critical isochore as was shown elsewhere [7]. Similarly to $\alpha_{p,max}$, the line of $c_{p,max}$ at constant pressure passes through a maximum at about $\rho = 1.65\rho_c$ [Fig. 3(c)]. In the p - T projection, the lines of the maxima of β_T and c_p at constant temperature [Fig. 3(b)] correspond to an increase in pressure with temperature increase, whereas the

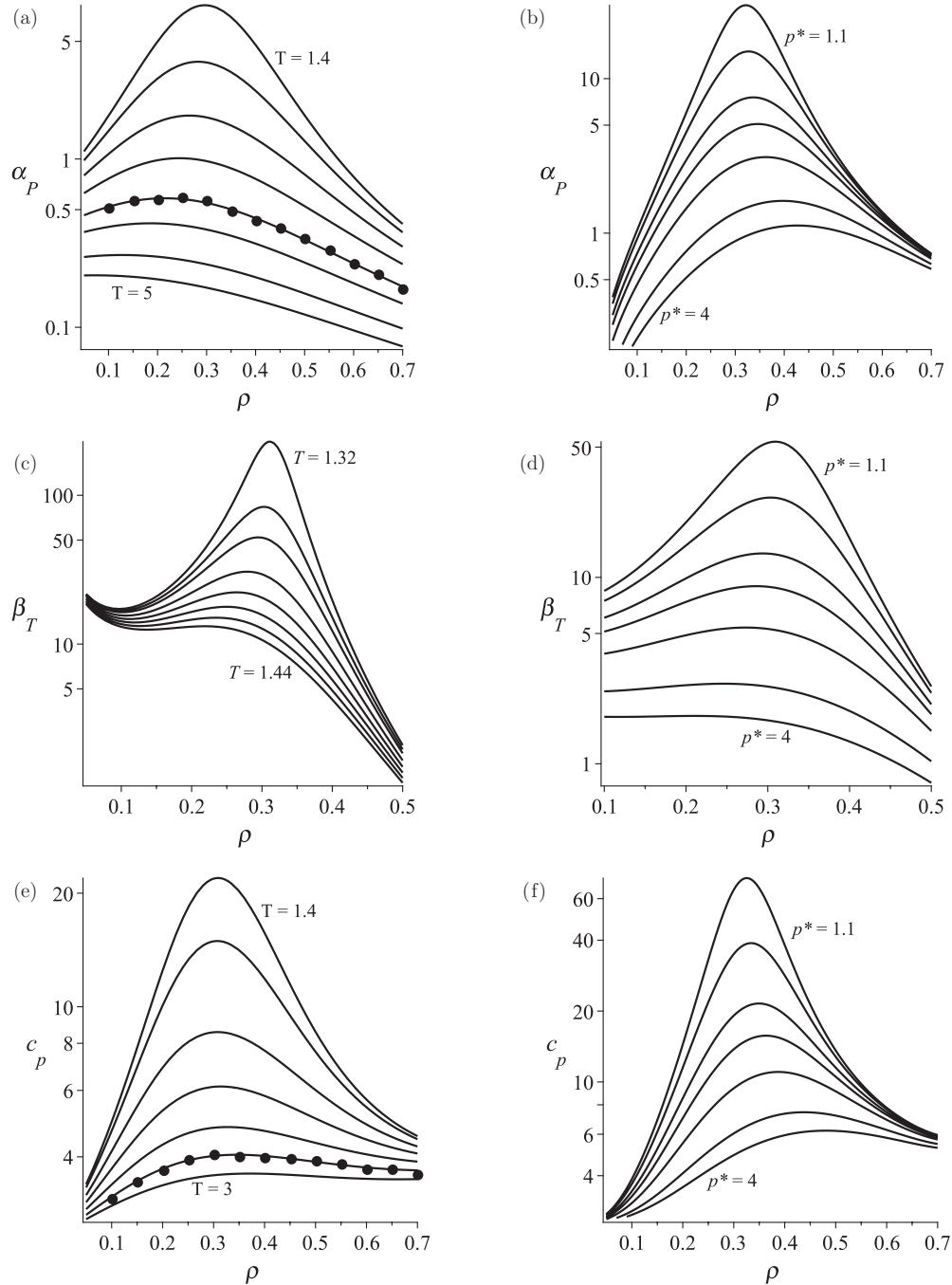


FIG. 2. Thermodynamic response functions of the LJ fluid: Thermal expansion coefficient α_P as a function of density ρ at (a) different constant temperatures $T = 1.4, 1.5, 1.7, 2, 2.5, 3, 4,$ and 5 (from top to bottom) and at (b) different constant pressures $p = p^* p_c$ with $p^* = 1.1, 1.2, 1.4, 1.6, 2, 3,$ and 4 (from top to bottom). Isothermal compressibility β_T as a function of density ρ at (c) different constant temperatures $T = 1.32, 1.33, 1.34, 1.36, 1.38, 1.4, 1.42,$ and 1.44 (from top to bottom) and at (d) different constant pressures as in (b). Isobaric heat capacity c_p as a function of density ρ at (e) different constant temperatures $T = 1.4, 1.45, 1.6, 1.8, 2.1, 2.5,$ and 3 (from top to bottom) and at (f) different constant pressures as in (b). The solid circles in (a) and (e) show results from the *NVEPG* ensemble method [20–22].

$\alpha_{P,\max}$ line changes its behavior at a temperature of about $T = 2.5 T_c$. The lines of maxima of α_P , c_p , and β_T at constant pressure [Fig. 3(d)] first correspond in all three cases to an increase in pressure with temperature increase, but then, in contrast to the behavior at constant temperature [Fig. 3(b)], $c_{p,\max}$ and $\alpha_{P,\max}$ pass through a maximum at higher pressure.

It is well known [13] that the use of different EOSs can cause different courses of extrema lines. We compared our results with those of the KN EOS [14]. The results for the lines of maxima of α_P , β_T , and c_p obtained from the KN EOS are shown as solid symbols in Figs. 3(c) and 3(d). The agreement between the two EOSs is very good, although the ansatz functions for them are very different, and it especially

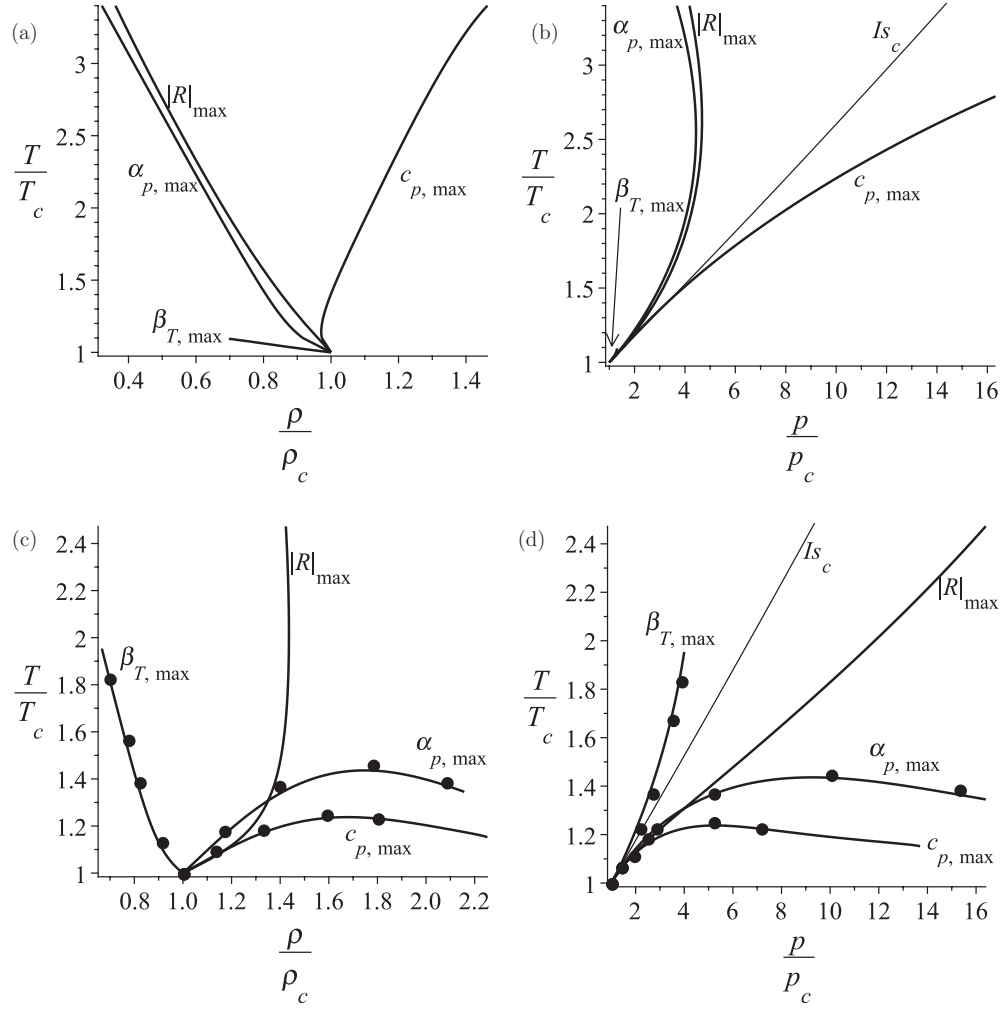


FIG. 3. (a),(b) Lines of maxima at constant temperature of the LJ fluid for the thermal expansion coefficient α_p , isothermal compressibility β_T , isobaric heat capacity c_p , and Riemannian thermodynamic scalar curvature R in the ρ - T phase diagram (a) and the p - T phase diagram (b). (c),(d) Lines of maxima at constant pressure of the LJ fluid for the thermal expansion coefficient α_p , isothermal compressibility β_T , isobaric heat capacity c_p , and Riemannian thermodynamic scalar curvature in the ρ - T phase diagram (c) and the p - T phase diagram (d). The solid circles are calculated from the Kolafa-Nezbeda EOS [14]. Is_c denotes the critical isochore.

suggests that the course of the line of maxima of c_p is not an artifact of the MBWR EOS.

We also compared the response functions calculated from the MBWR EOS with *NVEPG* ensemble simulation data [20–22]; from this method thermodynamic derivatives could be obtained directly. Since these calculations are very CPU intensive, we present results for only one isotherm. The isotherm at $T = 2.5$ was chosen, because at this temperature there are greater differences from other studies [7]. The values for α_p and c_p at $T = 2.5$ are shown as solid circles in Figs. 2(a) and 2(e). The difference between the two methods is less than 1.3% for c_p and less than 3.5% for α_p ; this indicates the high quality of the EOS.

IV. RIEMANNIAN THERMODYNAMIC SCALAR CURVATURE R AND THE WIDOM LINE

The Widom line is defined by the locus of points of maximum correlation length ξ . In a recent paper, Ruppeiner

et al. [8] established a new method for the construction of the Widom line based on the relation $|R| \sim \xi^3$ [9] between the Riemannian thermodynamic scalar curvature R and the volume of the correlation length. Therefore, the Widom line can be constructed from the maximum of $|R|$ where R is calculated from the thermodynamic metric.

If we use as before ρ - T coordinates as state variables, then the metric for these coordinates is diagonal, and the line element $d\ell$ which characterizes the distance between two neighboring thermodynamic states simply becomes [16]

$$d\ell^2 = g_{TT}dT^2 + g_{\rho\rho}d\rho^2. \quad (6)$$

We calculated the metric elements by using the free Helmholtz energy $f = u - Ts$, where u is the internal energy given by

$$u = \frac{3}{2}T + u^E \quad (7)$$

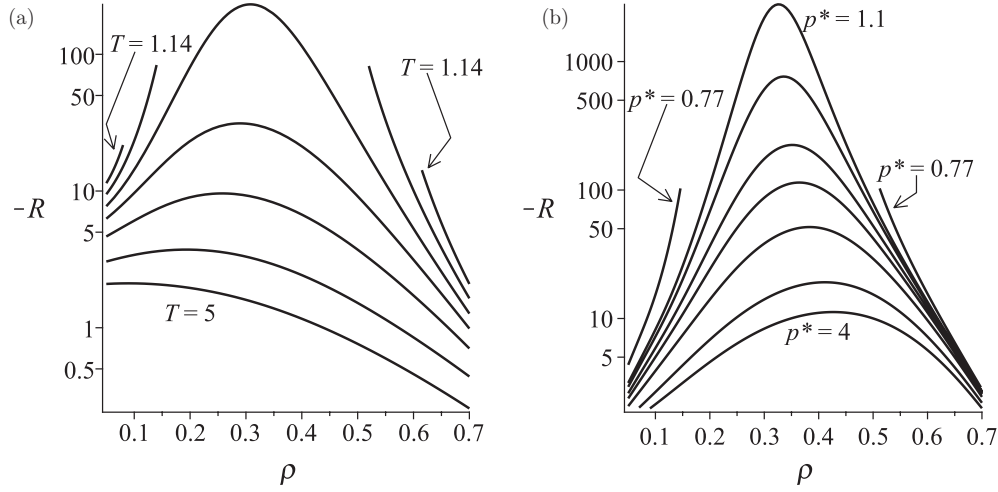


FIG. 4. Riemannian thermodynamic scalar curvature R of the LJ fluid: (a) $-R$ as a function of density at different constant temperatures $T = 1.14, 1.25, 1.4, 1.6, 2, 3,$ and 5 (from top to bottom). The curves are broken at the vapor-liquid coexistence line. (b) $-R$ as a function of density at different constant pressures $p = p^* p_c$ with $p^* = 0.7, 1.1, 1.2, 1.4, 1.6, 2, 3,$ and 4 (from top to bottom).

and s is the entropy, which can be calculated from (compare [23])

$$s = \frac{3}{2} \ln T - \ln \rho - \int_0^\rho \left(\frac{\partial p}{\partial T} - \rho \right) \frac{d\rho}{\rho^2}. \quad (8)$$

$f, u,$ and s are dimensionless quantities per particle. The metric elements are

$$g_{TT} = -\frac{1}{T} \frac{\partial^2}{\partial T^2} (\rho f), \quad (9)$$

$$g_{\rho\rho} = \frac{1}{T} \frac{\partial^2}{\partial \rho^2} (\rho f). \quad (10)$$

The determinant g of the metric tensor becomes

$$g = g_{TT} g_{\rho\rho} \quad (11)$$

and the Riemannian thermodynamic scalar curvature R is

$$R = \frac{1}{\sqrt{g}} \left[\frac{\partial}{\partial T} \left(\frac{1}{\sqrt{g}} \frac{\partial g_{\rho\rho}}{\partial T} \right) + \frac{\partial}{\partial \rho} \left(\frac{1}{\sqrt{g}} \frac{\partial g_{TT}}{\partial \rho} \right) \right]. \quad (12)$$

In our notation, R is a dimensionless quantity.

In Fig. 4 the density dependence of $-R$ at constant temperature [Fig. 4(a)] and at constant pressure [Fig. 4(b)] is given. A logarithmic scale is used because $-R$ strongly increases near the critical point, where it becomes singular. As can be seen from Fig. 4(a), the maximum vanishes for constant temperature near $T \approx 5$. Everywhere in the phase region of Fig. 4, $R < 0$. Ruppeiner [16] indicates that attractive interactions dominate if R is negative. It is a well-known fact that the vapor-liquid transition is dominated by attractive interactions whereas the fluid-solid transition is dominated by repulsion, and, indeed, R becomes positive for the LJ fluid on approaching the solid region. A detailed analysis of this transition based on the Riemannian geometry is in preparation.

In a similar way to the response functions, the extrema of the curves in Fig. 4 determine the line of curvature maxima, thus indicating the loci of correlation length maxima, e.g., the Widom line. In Fig. 3 we show the slope of $|R|_{\max}$ at

constant temperature and constant pressure in the ρ - T and p - T phase diagrams. The line of maxima of $|R|$ always starts at the critical point with a gradient very close to the gradient of the line of $c_{p,\max}$ in all projections of the phase space. But the curves of $|R|_{\max}$ and $c_{p,\max}$ move away from each other when the temperature is increased. The lines of maxima of $|R|$ at constant temperature [Figs. 3(a) and 3(b)] closely follow the line of $\alpha_{p,\max}$, whereas at constant pressure [Figs. 3(c) and 3(d)] the R_{\max} line crosses the $\alpha_{p,\max}$ line.

As a comparison, we also analyzed the vdW fluid. The reference temperature is now the critical temperature T_c , the reference density is the critical density ρ_c , the reference energy is $k_B T_c$, and the dimensionless pressure as a function of dimensionless density and temperature becomes

$$p = \frac{3}{8} \frac{\rho}{3 - \rho} (8T - 9\rho + 3\rho^2), \quad (13)$$

and the dimensionless internal energy per particle is

$$u = \frac{3}{2} T - \frac{9}{8} \rho. \quad (14)$$

We show the course of the ridges for α_p , β_T , and c_p as well as those of $|R|$ for a vdW fluid in the ρ - T and the p - T projections at constant temperature [Figs. 5(a) and 5(b)] and at constant pressure [Figs. 5(c) and 5(d)]. Obviously, there are differences between the two fluids, e.g., the slope of $c_{p,\max}$ at constant temperature follows the critical isochore in the ρ - T phase diagram in contrast to its behavior in the LJ fluid [compare Figs. 3(a) and 5(a)]. Furthermore, the slope of the $|R|_{\max}$ line closely follows the $\alpha_{p,\max}$ line for the LJ fluid at constant temperature in the ρ - T plane but not for the vdW fluid [compare Figs. 3(a) and 5(a)]. The loci of $\alpha_{p,\max}$ and $c_{p,\max}$ at constant pressure describe a right turn for the LJ fluid [Figs. 3(c) and 3(d)] which is very different from the behavior in the vdW fluid [Figs. 5(c) and 5(d)].

But there are some obvious similarities between the slopes of the $|R|_{\max}$ line for the LJ fluid and the vdW fluid. The slope of the $|R|_{\max}$ line does not follow the slope of any quantity that is shown in Fig. 3 or Fig. 5 except very near to the critical

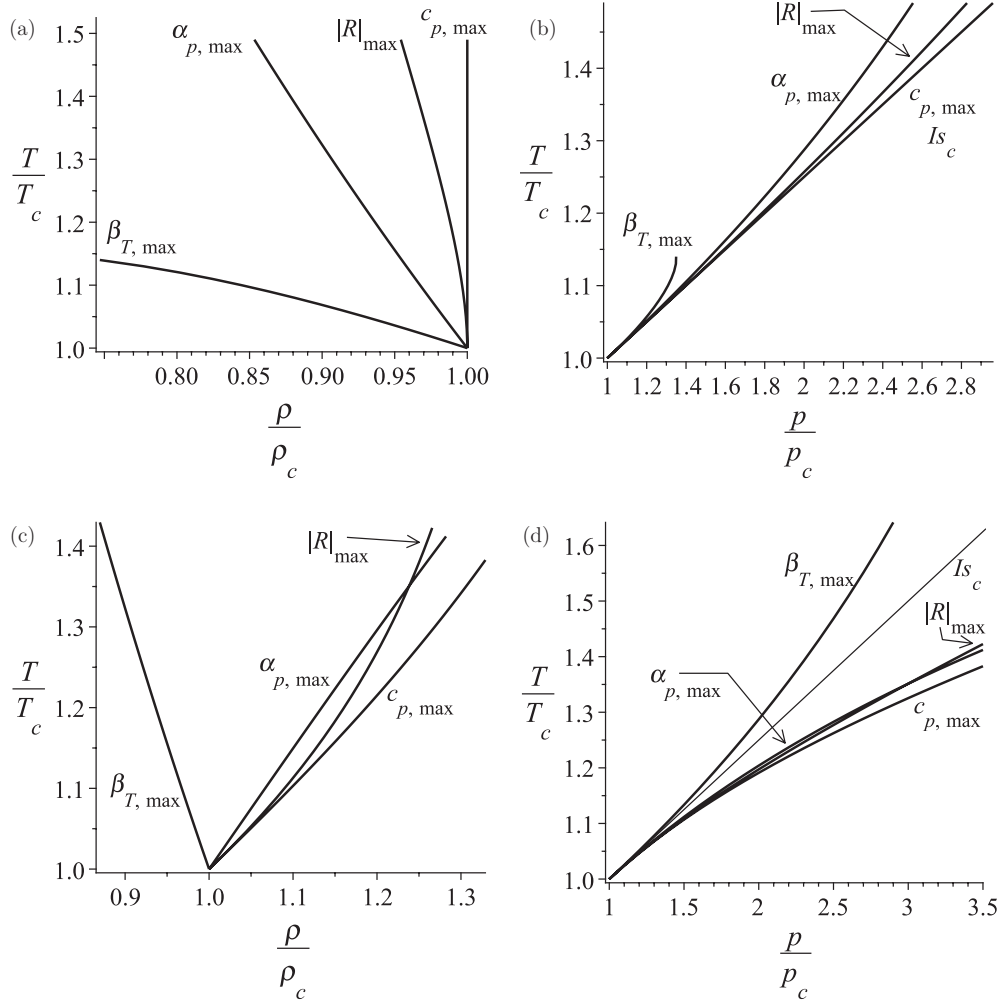


FIG. 5. (a),(b) Lines of maxima at constant temperature of the vdW fluid for the thermal expansion coefficient α_p , isothermal compressibility β_T , isobaric heat capacity c_p , and Riemannian thermodynamic scalar curvature $|R|$ in the ρ - T phase diagram (a) and the p - T phase diagram (b). (c),(d) Lines of maxima at constant pressure of the vdW fluid for the thermal expansion coefficient α_p , isothermal compressibility β_T , isobaric heat capacity c_p , and Riemannian thermodynamic scalar curvature in the ρ - T phase diagram (c) and the p - T phase diagram (d). Is_c denotes the critical isochore; the critical isochore lies on the $c_{p,\max}$ line in (b).

point, where the gradients are very close to those of the $c_{p,\max}$ line in all projections. The line of the maxima of $|R|$ at constant temperature [Fig. 5(a)] corresponds to a decrease in the density with temperature increase and is situated between the $\alpha_{p,\max}$ and $c_{p,\max}$ lines in the ρ - T phase diagram. The line of the maxima of $|R|$ at constant pressure [Figs. 5(c) and 5(d)] crosses the $\alpha_{p,\max}$ line for both the LJ fluid and the vdW fluid in the ρ - T and the p - T phase diagrams. In summary, we can say that there are obvious differences in the behavior of the response function maxima between the LJ and the vdW fluids; there are similarities, especially in the behavior of the scalar curvature maxima.

V. CALCULATION OF VAPOR-LIQUID PHASE EQUILIBRIA BY USE OF THE R -CROSSING METHOD

In addition to predicting the Widom line, Ruppeiner *et al.* [8] also provided a novel way of characterizing a first-order phase transition from a microscopic description based on

Riemannian geometry. The method connects density fluctuations and the width of the interface between the coexisting phases. Since the correlation length in the two phases must be the same and because of $|R| \sim \xi^3$, the coexistence curve of a first-order phase transition can be constructed from the fact that the Riemannian thermodynamic scalar curvature must be equal in the two coexisting phases.

In this study, we applied this idea to predict the vapor-liquid coexistence curve of a LJ fluid. In the preceding section, we described how to calculate the course of R along an isotherm for the vapor and the liquid regions. The corresponding pressure where the curvature curves cross each other can then be interpreted as the saturation pressure. Consequently, Ruppeiner *et al.* [8] called the procedure the R -crossing method. From this, the vapor-liquid equilibrium phase diagram can be constructed. We varied the pressure at a fixed temperature to get two slopes for R , a gas slope and a liquid slope; the pressure value where the R values are equal is taken as the reduced saturation pressure.

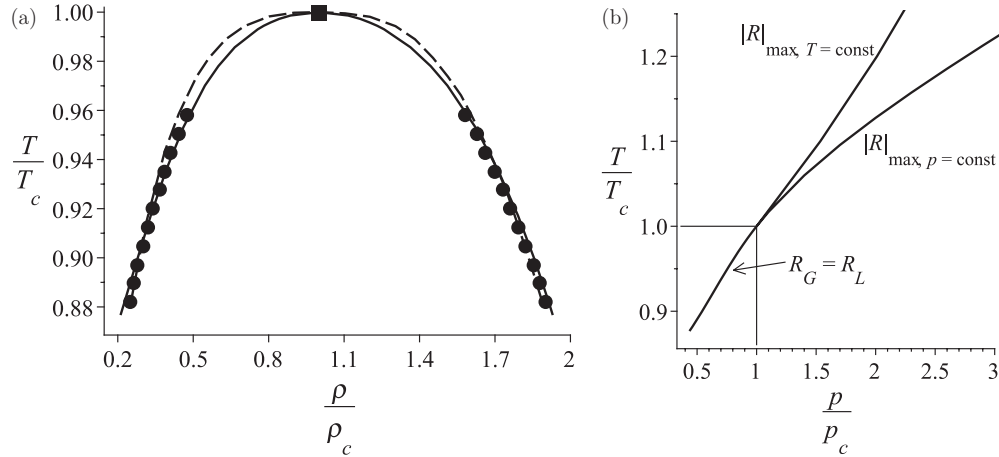


FIG. 6. (a) Vapor-liquid coexistence line in the ρ - T phase diagram. The continuous line is calculated with the R -crossing method, the symbols are simulation results of Shi and Johnson [18], and the dashed line is calculated from an Ising-form power law [18]. The lines start where $|R_G| \rho_G = 1$. (b) p - T phase diagram.

In Fig. 6(a) we compare the vapor-liquid coexistence curve obtained from the R -crossing method (solid line) with those of simulation results (symbols) [18] and a fit of an Ising-form power law (dashed line) [18] in the density-temperature projection of the phase space. The simulation results of Shi and Johnson [18] were obtained from a long-range corrected LJ potential with a reduced cutoff value of 5 by using multiple histogram reweighting. The method is considered to be accurate and effective for computing phase diagrams. The histogram data were collected from grand canonical Monte Carlo simulations [18]. The overall agreement between the results of the R -crossing method and the simulation results is very good. The Ising power law expression is given by

$$\rho_{\pm} - \rho_c = a|T - T_c| \pm b|T - T_c|^{\beta}, \quad (15)$$

where ρ_+ is the liquid density, ρ_- is the vapor density, and β is the critical exponent. The fit result is taken from the

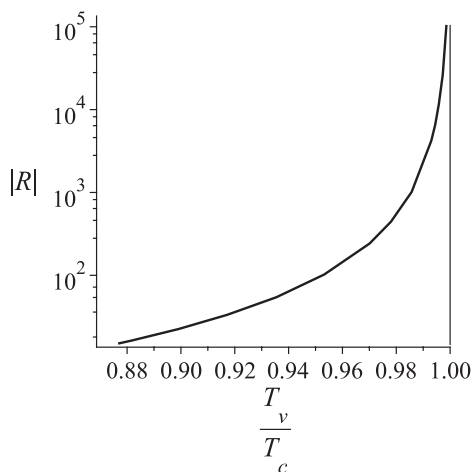


FIG. 7. Riemannian thermodynamic scalar curvature R of the LJ fluid as a function of the evaporation temperature T_v along the coexistence line. The R values are equal for the gas and the liquid phases.

paper of Shi and Johnson [18]. In particular, the results of the R -crossing method follow the curvature of the coexistence line obtained from simulation data well; this results in a narrowing of the phase envelope in the vicinity of the critical point compared to the fit of an Ising-form power law.

In Fig. 6(b) we show the vapor-liquid coexistence line in the p - T projection of the phase space. The extension of this line into the supercritical region, i.e., the Widom line, is shown for the $|R|$ maximum at constant temperature and constant pressure. Obviously, the slope of $|R|_{\max}$ at constant temperature increases more rapidly upon compression than does the slope of $|R|_{\max}$ at constant pressure.

Despite the striking agreement, the R -crossing method is not free of limitations. In this approach, the correlation volume ξ^3 should be large enough to encompass a number of atoms adequate for a thermodynamic approach. A good estimate for the validity of the R -crossing method is the relation $|R_G|/v_G \sim 1$, where v_G is the coexistence molecular volume in the vapour phase. For $|R_G|/v_G \geq 1$, the method is strictly valid [8]. In Fig. 6, the coexistence curve (solid line) starts where the condition $|R_G|/v_G = 1$ is met.

Figure 7 shows the Riemannian thermodynamic scalar curvature of the LJ fluid along the coexistence line as a function of T_v/T_c , where T_v is the evaporation temperature. The curvature becomes singular at the critical point, thus indicating that the correlation length diverges.

VI. CONCLUSIONS

In this study, we have analyzed in detail the supercritical behavior of thermodynamic response functions for a LJ system. We calculated a new parameter set for the MBWR EOS based on an extensive set of simulation data of 348 state points. From the EOS we constructed the course of slopes of maxima at constant temperature and constant pressure for the isothermal compressibility β_T , the isobaric heat capacity c_p , and the thermal expansion coefficient α_p in the phase space. The lines of extrema were used recently to estimate the so-called Widom line under the assumption that the

ridges of β_T , c_p , and α_P merge into one single line in the vicinity of the critical point. We showed that this assumption is limited because the bunch of ridges widens rapidly upon departure from the critical point. Following the new approach of Ruppeiner *et al.* [8], we constructed the Widom line for a LJ fluid without any use of response function extrema. We estimated the Widom line by calculating the thermodynamic scalar curvature R from the new fit of the MBWR EOS; the curvature is related to the volume of the correlation length ξ by $|R| \sim \xi^3$. The Widom line of the LJ fluid does not follow the slope of any response function extrema except in the vicinity of the critical point. Here, the Widom line closely follows the slope of the $c_{p,\max}$ line, but then it immediately runs away from the loci of $c_{p,\max}$ in the supercritical region.

Following the approach of Ruppeiner *et al.*, we also constructed the vapor-liquid coexistence line for the LJ fluid

based on the R -crossing method. The method uses the idea of characterizing liquid-gas phase transitions by the equality of the correlation lengths in the coexisting phases; this implies continuity at the phase boundary of the thermodynamic scalar curvature. We compared our results for the coexistence line with those of simulation data where multiple histogram reweighting was used to predict the phase envelope. We found striking agreement between the two methods, thus supporting the power of the Riemannian geometry description for these problems.

ACKNOWLEDGMENTS

We wish to thank Professor George Ruppeiner for helpful hints and we thank Alexander May for the preparation of some data files.

-
- [1] R. J. Bearman, B. C. Freasier, and D. K. Smith, *J. Phys. Chem.* **96**, 4093 (1992).
 - [2] B. C. Freasier and R. J. Bearman, *J. Chem. Phys.* **100**, 3094 (1994).
 - [3] B. C. Freasier, C. E. Woodward, and R. J. Bearman, *J. Chem. Phys.* **106**, 10318 (1997).
 - [4] D. Boda, T. Lukacs, J. Liszi, and I. Szalai, *Fluid Phase Equilib.* **119**, 1 (1996).
 - [5] M. M. Pineiro, C. A. Cerdeirina, and M. Medeiros, *J. Chem. Phys.* **129**, 014511 (2008).
 - [6] G. G. Simeoni, T. Bryk, F. A. Gorelli, M. Krisch, G. Ruocco, M. Santoro, and T. Scopigno, *Nat. Phys.* **6**, 503 (2010).
 - [7] V. V. Brazhkin, Y. D. Fomin, A. G. Lyapin, V. N. Ryzhov, and E. N. Tsiok, *J. Phys. Chem. B* **115**, 14112 (2011).
 - [8] G. Ruppeiner, A. Sahay, T. Sarkar, and G. Sengupta, e-print arXiv:1106.2270.
 - [9] G. Ruppeiner, *Rev. Mod. Phys.* **67**, 605 (1995); **68**, 313(E) (1996).
 - [10] J. J. Nicolas, K. E. Gubbins, W. B. Streett, and D. J. Tildesley, *Mol. Phys.* **37**, 1429 (1979).
 - [11] J. K. Johnson, J. A. Zollweg, and K. E. Gubbins, *Mol. Phys.* **78**, 591 (1993).
 - [12] K. Meier, Ph.D. thesis, University of the Federal Armed Forces, Hamburg, 2002.
 - [13] J. Gregorowicz, J. P. O'Connell, and C. J. Peters, *Fluid Phase Equilib.* **116**, 94 (1996).
 - [14] J. Kolafa and I. Nezbeda, *Fluid Phase Equilib.* **100**, 1 (1994).
 - [15] V. V. Brazhkin and V. N. Ryzhov, *J. Chem. Phys.* **135**, 084503 (2011).
 - [16] G. Ruppeiner, *Am. J. Phys.* **78**, 1170 (2010).
 - [17] G. Ruppeiner, *Phys. Rev. E* **72**, 016120 (2005).
 - [18] W. Shi and J. K. Johnson, *Fluid Phase Equilib.* **187–188**, 171 (2001).
 - [19] P. Mausbach and H.-O. May, *Fluid Phase Equilib.* **214**, 1 (2003).
 - [20] R. Lustig, *J. Chem. Phys.* **100**, 3048 (1994).
 - [21] K. Meier and S. Kabelac, *J. Chem. Phys.* **124**, 064104 (2006).
 - [22] P. Mausbach and R. J. Sadus, *J. Chem. Phys.* **134**, 114515 (2011).
 - [23] H.-O. May and P. Mausbach, *Fluid Phase Equilib.* **313**, 156 (2012).